

Transiting exoplanets from the CoRoT space mission[★]

XVII. The hot Jupiter CoRoT-17b: a very old planet

Sz. Csizmadia¹, C. Moutou², M. Deleuil², J. Cabrera^{1,3}, M. Fridlund⁴, D. Gandolfi⁴, S. Aigrain⁵, R. Alonso⁶, J.-M. Almenara², M. Auvergne⁷, A. Baglin⁷, P. Barge², A. S. Bonomo², P. Bordé⁸, F. Bouchy^{12,13}, H. Bruntt⁷, L. Carone¹⁴, S. Carpano⁴, C. Cavarroc⁸, W. Cochran⁹, H. J. Deeg^{10,11}, R. F. Díaz¹³, R. Dvorak¹⁵, M. Endl⁹, A. Erikson¹, S. Ferraz-Mello¹⁶, Th. Fruth¹, J.-C. Gazzano^{2,17}, M. Gillon¹⁸, E. W. Guenther¹⁹, T. Guillot¹⁷, A. Hatzes¹⁹, M. Havel¹⁷, G. Hébrard^{12,13}, E. Jehin¹⁸, L. Jorda², A. Léger⁸, A. Llebaria², H. Lammer²⁰, C. Lovis⁶, P. J. MacQueen⁹, T. Mazeh²¹, M. Ollivier⁸, M. Pätzold¹⁴, D. Queloz⁶, H. Rauer^{1,22}, D. Rouan⁷, A. Santerne², J. Schneider³, B. Tingley^{10,11}, R. Titz-Weider¹, and G. Wuchterl¹⁹

(Affiliations can be found after the references)

Received 3 April, 2011; accepted 27 April, 2011

ABSTRACT

We report on the discovery of a hot Jupiter-type exoplanet, CoRoT-17b, detected by the CoRoT satellite. It has a mass of $2.43 \pm 0.30 M_{\text{Jup}}$ and a radius of $1.02 \pm 0.07 R_{\text{Jup}}$, while its mean density is $2.82 \pm 0.38 \text{ g/cm}^3$. CoRoT-17b is in a circular orbit with a period of 3.7681 ± 0.0003 days. The host star is an old (10.7 ± 1.0 Gyr) main-sequence star, which makes it an intriguing object for planetary evolution studies. The planet's internal composition is not well constrained and can range from pure H/He to one that can contain ~ 380 earth masses of heavier elements.

Key words. stars: planetary systems - techniques: photometry - techniques: radial velocities - techniques: spectroscopic

1. Introduction

Similar to eclipsing binaries, which offer the "Royal Road" to understanding the physics and nature of stars (Russell 1932; Batten 2005), transiting exoplanets are key objects in terms of understanding the formation, evolution and properties of planets. In Russell's context, 'Royal Road' means that we have a way to obtain data that were previously unavailable by other observational methods (Batten 2005). The transits and - if they are observable - occultations of exoplanets provide unique possibilities to determine e.g. their mass, radius and orbital characteristics, atmospheric composition as well as internal structure. The consecutive transit and occultation observations allow us to study

the orbital element changes caused by either gravitational interaction with another body or by tidal and/or magnetic interactions between the star and the planet.

CoRoT (Convection, Rotation and planetary Transit) is a 27 cm diameter space-telescope (Baglin 2007). The goals of the mission are to obtain long-term photometric data sets for asteroseismological studies on relatively bright pulsating stars and to search for new transiting exoplanets. Here we report the detection of another hot Jupiter, named CoRoT-17b. It orbits a faint star ($V \approx 15.5$) in a 3.76 days orbit. As we will show below, the host star is evolved and quite old: its age is 10.7 ± 1.0 Gyr.

2. CoRoT observations and their analysis

2.1. Data

CoRoT-17 is located in the so-called LRC03 field, which was a medium-long field (for the target's coordinates see Table 1 and for the finding chart see Fig. 1)¹. The star is listed in many photometric catalogues (for a selection see Table 1), from which its spectral energy distribution is known from the optical to mid-infrared.

The star was observed for 89.2 days, from HJD 2 454 925.4199 to HJD 2 455 014.6107, corresponding to the period from 2009 April 03, 22 UT until 2009 July 02, 03 UT. In total, 14,861 data points were obtained in white light. However, some of these data points were obtained when the satellite

[★] The CoRoT space mission, launched on December 27th 2006, has been developed and is operated by CNES, with the contribution of Austria, Belgium, Brazil, ESA (RSSD and Science Programme), Germany and Spain. Part of the observations were obtained at the Canada-France-Hawaii Telescope (CFHT) which is operated by the National Research Council of Canada, the Institut National des Sciences de l'Univers of the Centre National de la Recherche Scientifique of France, and the University of Hawaii. Based on observations made with HARPS spectrograph on the 3.6-m European Organisation for Astronomical Research in the Southern Hemisphere telescope at La Silla Observatory, Chile (ESO program 184.C-0639). Based on observations made with the IAC80 telescope operated on the island of Tenerife by the Instituto de Astrofísica de Canarias in the Spanish Observatorio del Teide. Part of the data presented herein were obtained at the W.M. Keck Observatory, which is operated as a scientific partnership among the California Institute of Technology, the University of California and the National Aeronautics and Space Administration. The Observatory was made possible by the generous financial support of the W.M. Keck Foundation.

¹ The interested reader can find more details about the CoRoT observational strategy in Baglin et al. (2007), Boissard et al. (2006) and Auvergne et al. (2009).

Table 1. IDs, coordinates, and magnitudes of CoRoT-17.

CoRoT window ID	LRc03_E2_2182	
CoRoT ID	311519570	
2MASS	2MASS18344782-0636440	
UCAC3	3UC 167-181321	
USNO-A2	0825-12387389	
USNO-B1	0833-042306	
GSC 2.2	S3003-3212601	
GSC 2.3	S909002601	
NOMAD1	0833-0454552	
Coordinates		
RA (J2000)	18h 34m 47.82s	
Dec (J2000)	−6° 36′ 44.04″	
Magnitudes		
Filter	Mag & Error	Source
r′	15.346±0.007	ExoDat ^a
i′	14.521±0.011	ExoDat
V	15.46	ExoDat
J	13.174 ± 0.036	2MASS
H	12.615 ± 0.062	2MASS
K	12.472 ± 0.054	2MASS
[3.6]	12.232 ± 0.068	IRAC
[4.5]	12.181 ± 0.069	IRAC
[5.8]	12.149 ± 0.142	IRAC
[8.0]	12.079 ± 0.151	IRAC

Notes. ^(a) Deleuil et al. (2009)

crossed the so-called South Atlantic Anomaly (SAA), which causes an increase in the high-energy particle flux and strongly affects the observed fluxes. We excluded these data points as well as those that were flagged by the pipeline for other reasons (Baudin et al 2008). For instance, we excluded all data points that were acquired during the transition of the satellite from light to Earth-shadow (see Auvergne et al. 2009) or vice versa (779 and 795 data points, respectively). These transitions cause considerable voltage and temperature fluctuations (Auvergne 2009). We kept 10,489 good data points (71.4% of all the data points). The exposure time was uniformly 512 seconds for CoRoT-17b because of the faintness of the star.

The original observations were reduced by the CoRoT pipeline. The jumps, caused by high-energy particle impacts (cosmic ray events, see Auvergne et al 2009), were corrected by us. The result can be seen in Figure 2.

The light curve also shows some non-periodic modulation with an amplitude of $\sim 2\%$, probably caused by stellar activity. The spectroscopic analysis of the star (Sect. 3.3) yielded $v \sin i \approx 4.5 \pm 0.5$ km/s projected rotational velocity and the combined spectroscopic and photometric analysis of the stellar properties gave $R_{\text{star}} = 1.59R_{\odot}$ (Sect. 3.3). From this one can expect $P = 20.1$ days rotational period for the star. We calculated the Lomb-Scargle periodogram of the light curve, but no clear periodicity nor any peak in the periodogram relatively close to this expected value were found.

The transits were detected in the so-called ‘alarm-mode’ (Quentin et al. 2006 Surace et al. 2008). Twenty-five transit events were observed by CoRoT with an orbital period of 3.7681 days. These events are analysed in Sect. 2.2. The duration of the transit was measured to be 4.72 hours and its depth is approximately 0.44% (see Figure 3 and Table 2.).

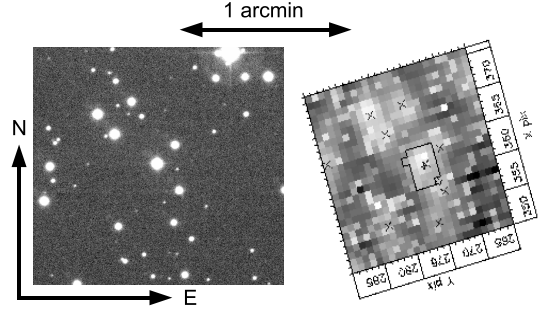


Fig. 1. Sky area around CoRoT-17 (star in the centre). Left: g-filter image with a resolution of $0.7''$ taken with the CFHT telescope. Right: image taken by CoRoT at the same scale and orientation. The jagged outline in its centre is the photometric aperture mask; indicated are also CoRoT’s x and y image coordinates and positions of nearby stars that are in the ExoDat database (Deleuil et al. 2009).

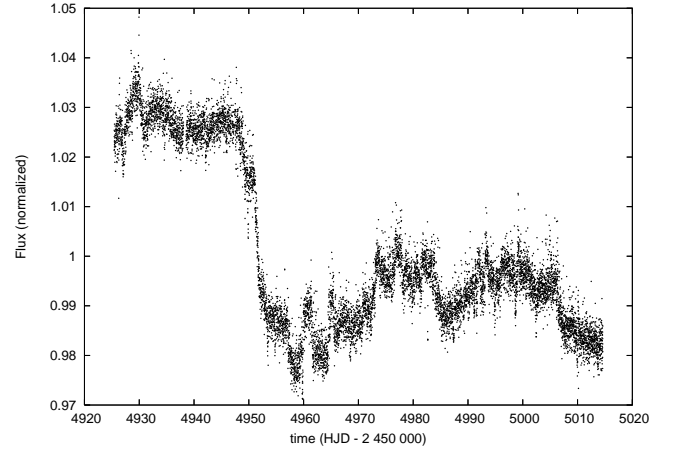


Fig. 2. Light curve of CoRoT-17 after removing the most obvious jumps.

2.2. Transit modelling

Owing to the very complicated nature of the light curve, which is affected by various instrumental effects such as jumps, SAA-crossing etc., we constructed the transit light curve for the modelling in the following way. We excluded transits 5, 8, 12, 18, and 24, which were strongly altered by instrumental effects. Then we folded the light curve as shown in Fig. 3.

The instant of the centre of the i th transit is obviously $T_i = T_0 + iP$. Preceding and following the beginning and the end of each transit, we cut one transit duration-long part of the light curve before and after the transit and fitted them by a parabola. Next, we selected the data points from the interval $T_i - 1.5D < t < T_i + 1.5D$ and then divided these light curve segments by the corresponding parabola. Here D is the duration of the transit. After that we removed outliers by applying a 5σ clipping. As a final step, we repeated this procedure again.

The transit light curve (Fig. 3) was fitted by a model to obtain the relevant geometrical and physical parameters of the system. We used the Mandel & Agol (2002) model and a specified genetic algorithm (Geem et al. 2001) for the transit fit. Genetic algorithms have already successfully been used to model the light

curves of eclipsing binary stars, and it was also applied to transit light curves (Fridlund et al 2010). Genetic algorithms have the advantage that it is possible to map the whole parameter space, therefore it is more likely to find the global minimum in the parameter hyperspace. The errors of the parameters can be easily estimated using a genetic algorithm approach, too. We give the 1σ -error bars, estimated from the width of the distribution of points, which are between χ_{min}^2 and $\chi_{min}^2 + 1$.

Our free parameters were: semi-major axis to the stellar radius ratio (a/R_{star}), planet-to-stellar radius ratio (k), impact parameter ($b = a \cos i / R_{star}$, where i is the inclination), and the combination of $u_+ = u_1 + u_2$, while we kept fixed $u_- = u_1 - u_2$. Here u_1 and u_2 are the linear and the quadratic limb-darkening coefficients, respectively. The usage of these combinations was suggested by Brown et al (2001) and they are widely used in the transit modelling studies.

The contamination factor was a free parameter as well. This parameter gives an estimate of the fraction of the total observed flux that comes from different stars and not from the target object, because of the large PSF of CoRot (Figure 1). Bordé et al (2010) described in detail how to determine this factor for CoRoT-targets. Applying the same method, we adopted $8 \pm 4\%$ for the contamination factor and it could vary within these constraints.

In total, we had five free parameters. Because the radial velocity curve indicates a probably circular orbit, we assumed that the eccentricity is zero for the light curve modelling.

We calculated 13 different models, each of which had a fixed, but different value of u_- . The fixed values of this combination of limb darkening coefficients were -0.3, -0.2, -0.1, ..., 0.7, 0.8 and 0.9. Convergence was reached after $\sim 40\,000$ iterations at every fixed u_- value. The “best” light curve solution was then defined as the “centre of gravity”-like average-value of the 1000 lowest χ^2 at every fixed u_- value.

The χ^2 -values showed an absolute minimum value at $u_- = 0.2$ where u_+ was equal to 0.65 ± 0.17 . We checked whether our limb-darkening coefficients agree with the theoretical ones, derived from the effective temperature, $\log g$ and metallicity of the star (see Sect. 3.3). Using the tables of Sing (2010), we found that theoretically they are $u_- = 0.23 \pm 0.03$ and $u_+ = 0.68 \pm 0.03$ for CoRoT-17. (The uncertainties of the theoretical values stem from the uncertainties of the stellar parameters.) The modelled values are close to this prediction. We do not investigate this problem further, because the photometric signal-to-noise ratio is not sufficient to determine both limb-darkening coefficients simultaneously, and because the found best value was within the error bars of the predicted one, the agreement is satisfactory. The finally adopted solution is shown in Fig. 3. The results of the transit light curve modelling is given in Table 2. In the subsequent analysis we need the $M_{star}^{1/3}/R_{star}$ for the determination of the stellar mass and radius. Re-arranging Kepler’s third law (Roberts 1899; Winn 2010), we calculate a value for this quantity of 0.61 ± 0.03 (solar units).

2.3. Parameter correlations

The result of transit lightcurve modelling can be degenerate, leading to equally acceptable solutions. For CoRoT-3b, for instance, the light curve modelling itself showed that in the inclination - limb darkening coefficient plane there are two solutions, which cannot be distinguished from each other (Deleuil et al. 2008). It was already noticed in Brown et al. (2001) that at low impact parameters the solutions are degenerate in the

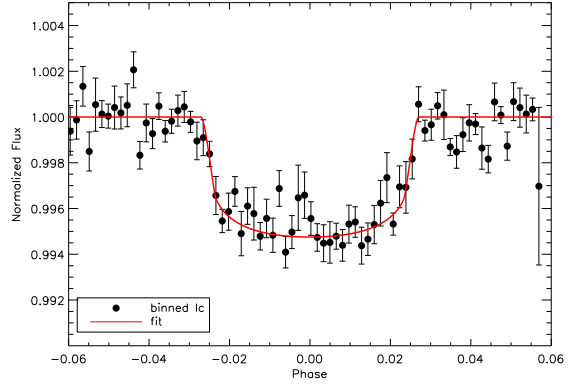


Fig. 3. Light curve solution of CoRoT-17. For the sake of clarity, we superimposed the fit (red line) on the binned data instead of the original ones. The features on the bottom of the light curve (sudden flux increases) maybe caused by some spot crossing.

inclination-limb darkening coefficient plane if the observational errors are relatively large. Because CoRoT-17 is relatively faint, the light curve modelling most likely forms an ill-posed problem because of the noise levels involved. Therefore it is important to investigate how the various derived parameters are correlated.

To do that, we selected six combinations of four free parameters (a/R_{star} , k , b and u_+ , see Fig. 4). Each of these combinations consisted of two parameters. Then we fixed the other parameters at their values given in Table 2 determined before, while several hundreds of randomly selected combinations of the two investigated parameters were varied over a large interval of values. The panels of Fig. 4 show the models within 1σ (red), 2σ (green) and 3σ (blue).

We found that a/R_{star} and k are not correlated, while we found negligible correlation for the pair of $a/R_{star} - u_+$, and the correlation between $k - u_+$ is moderate. It is remarkable that the $k - b$ and $b - u_+$ diagram has a non-symmetrical distribution. The well-known correlation between a/R_{star} and the impact parameter b can also be seen. From the top right panel of Fig. 4 we can only give wide limits for these two parameters.

Studying these correlation diagrams, we concluded that all the parameters are well determined and unique, but the semi-major axis and the impact parameter are correlated. An impact parameter between 0 and 0.3 is the most probable value, but we are not able to constrain it better from the presently available photometry. It is safer to state that the semi-major axis/stellar radius ratio is most probable between 6.0–6.4, but it is also hard to give better constraints. To gain more precise values one requires even more precise photometry for this faint star.

3. Ground-based observations and their analysis

3.1. Photometric measurements

As part of the ground-based photometric follow-up programme of CoRoT candidates, observations of CoRoT-17 were undertaken from several telescopes. The aim of these observations was to assess if the transit-events observed by CoRoT really arise from the CoRoT target star and not from any contaminating nearby variable source. For more details on this follow-up programme, its motivation, techniques and results, see Deeg et al. (2009).

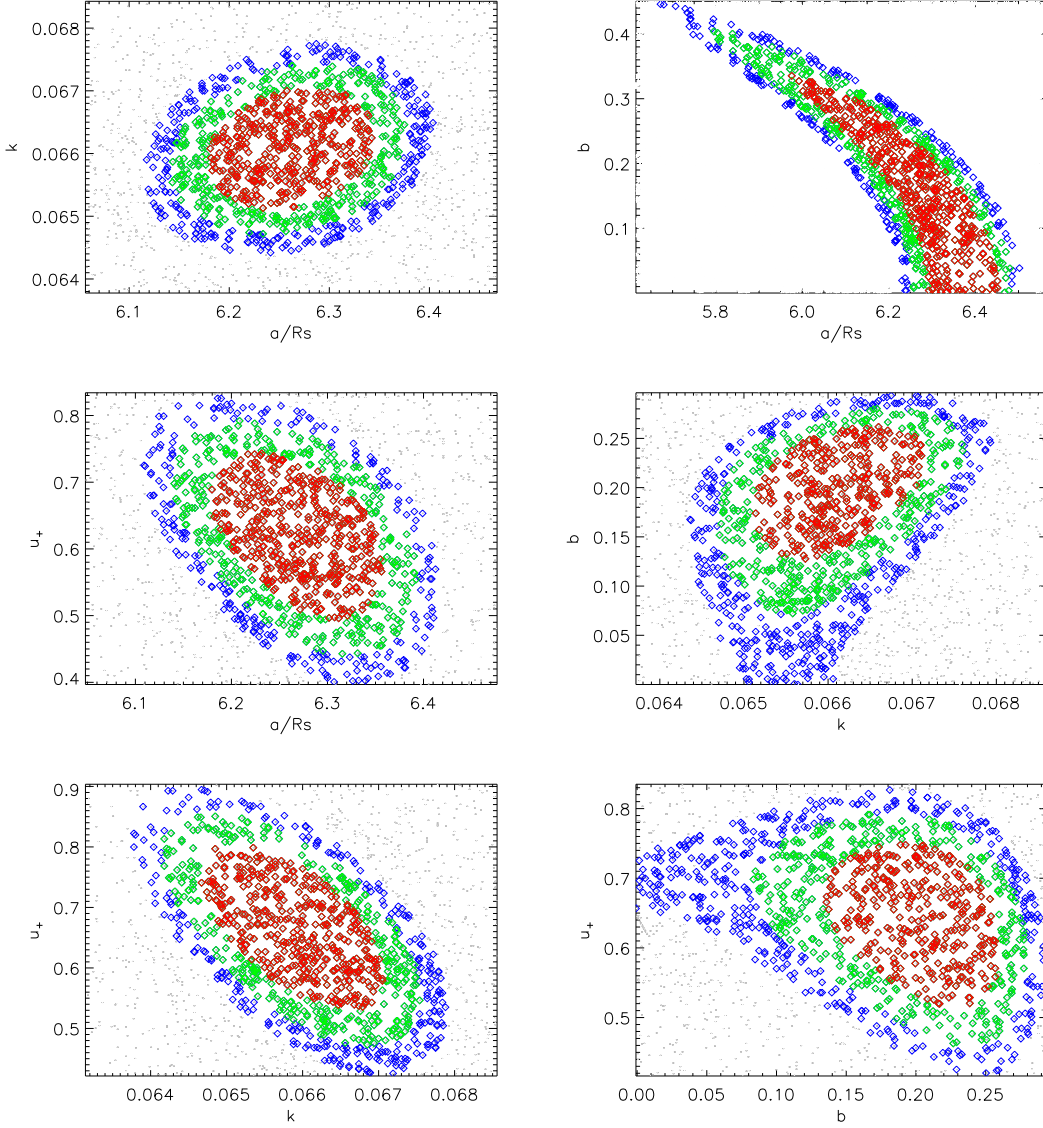


Fig. 4. Parameter-correlation diagrams for CoRoT-17.

Table 3. Telescopes used to assess the transit events observed by CoRoT and the log of observations. See text for discussion. For TRAPPIST see Gillon et al. (2011) while for BEST II see Erikson et al. (2011).

Telescope	Date of observation	Note
CFHT/MEGACAM	2010 May 17	ON/OFF
	2010 June 5	ON/OFF
OGS (Tenerife)	2010 June 9	ON
	2010 June 10	OFF
TRAPPIST (La Silla)	2010 May 24	Only egress phase was observed
BEST II (Cerro Armazones)	2010 June 5	Photometry during the full event

The log of observations and the list of the used telescopes can be found in Table 3. Of these observations, none showed any sign of relevant variability on any of several stars that are contaminating the CoRoT-aperture (Fig. 1). These stars would have to display eclipses with amplitudes of at least 7%, which would have been detected by any of the ground-observations that were undertaken. Only the second night from CFHT on 2010 June 5 also showed a significant variation on the target itself with an amplitude of 0.55%, close to the expected one from CoRoT.

The absence of a signal from the target in the other data has the following reasons: (i) the observations obtained in May suffered from a preliminary ephemeris and thus they did not see the deepest part of the transit. As a result of this experience, the ephemeris was refined and replaced in early June, 2010. (ii) The transit event in June was too shallow for OGS and BEST II and that is why these data were used only to exclude possible background eclipsing binaries.

Table 2. Physical and geometrical parameters of the CoRoT-17 system. Inclination (i) was calculated from the a/R_{star} ratio and from the impact parameter b . The parameter $M^{1/3}/R$ can be calculated from the orbital period and from the a/R_{star} value (see e.g. Winn 2010). T_{eq} is the equilibrium temperature of the planet.

Determined from photometry	
Epoch of periastron T_0 [HJD-2400000]	$54\,923.3093 \pm 0.0036$
Orbital period (days)	3.7681 ± 0.0003
Duration of the transit (hours)	4.72
Depth of the transit (%)	0.44
Determined from RV-measurements	
Orbital eccentricity e	0 [fixed]
Argument of periastron ω [deg]	0 [fixed]
Radial velocity semi-amplitude K [m s^{-1}]	312.4 ± 29.0
Systemic velocity V_γ [km s^{-1}]	54.770 ± 0.008
O-C residuals [m s^{-1}]	77
Determined from spectral analysis of the star	
T_{eff} [K]	5740 ± 80
$\log g_{\text{star}}$ [cgs]	4.40 ± 0.10
$[Fe/H]$	0.0 ± 0.1
$v \sin i$ [km s^{-1}]	4.5 ± 0.5
Spectral type	G2V
Determined from light curve modelling	
a/R_{star}	6.23 ± 0.24
b	0.18 ± 0.16
i [deg]	88.34 ± 1.54
k	0.0661 ± 0.0019
u_+	0.65 ± 0.17
u_-	0.2 (fixed)
Combined results	
Stellar mean density ρ_{st} [solar]	0.23 ± 0.02
Stellar mass M_{st} [solar]	1.04 ± 0.10
Stellar radius R_{st} [solar]	1.59 ± 0.07
Stellar age [Gyrs]	10.7 ± 1.0
Orbital semi-major axis a [AU]	0.0461 ± 0.0008
Planet mass M_p [M_J]	2.43 ± 0.30
Planet radius R_p [R_J]	1.02 ± 0.07
Planet mean density ρ_p [g cm^{-3}]	2.82 ± 0.38
$M_{\text{st}}^{1/3}/R_{\text{st}}$ [solar units]	0.61 ± 0.03
T_{eq} [K]	1626 ± 31
Distance [pc]	920 ± 50
A_V [mag]	2.60 ± 0.10

In conclusion, the absence of variability in the brighter contaminating stars as well as the detection of a correct brightness-variation on the target assured that the signal observed by CoRoT really arose from the target.

3.2. Radial velocity measurements and orbit of CoRoT-17b

HARPS is used to establish the planetary nature of CoRoT candidates and to identify binaries, in coordination with SOPHIE at Observatoire de Haute-Provence and HIRES at the Keck telescope (Bouchy, Moutou and Queloz, 2009). For radial velocity measurements of CoRoT-17, we used only HARPS (Mayor et al 2003). RV positions are estimated by cross-correlation of the stellar spectrum with a numerical mask (Baranne et al 1996, Pepe et al 2003). It commonly reaches uncertainties of 1 m/s on bright stars, up to typically 50-100 m/s for a $V \approx 15.5$ as CoRoT-17.

Between May and August, 2010, CoRoT-17 has been observed with HARPS at a spectral resolution of 110,000, together with a simultaneous on-sky reference in fiber B for monitoring the sky background. In total, seventeen measurements have

been secured. Some measurements have been acquired when the moon was up, but the velocity difference between the stellar spectrum and the barycentric Earth RV is always larger than 22 km/s, so that the stellar cross-correlation function is not significantly contaminated. Hence, the RV measurements have not been corrected for, even when the sky background is detected. With an exposure time of 1 hour, a typical signal-to-noise ratio of 8 is achieved on this target. The average uncertainty of the derived velocities is 74 m/s (see Table 4).

The *rms* of the RV time series is 244 m/s, indicating a fluctuation three times higher than the error bars (Fig. 5). When phased at the CoRoT period and transit ephemeris, a sinusoidal variation is clearly observed (Fig. 6), characterized by a semi-amplitude $K = 312$ m/s and systemic velocity $V_0 = 54.8$ km/s. The cross-correlation function is narrow ($FWHM = 9.6$ km/s), typical of a main-sequence slow-rotating star. The estimated projected velocity of the star is 5 ± 1 km/s (this value is slightly refined in the next paragraph, using the co-added spectra). The Keplerian solution is shown in Figures 5 and 6, where the orbital eccentricity is fixed to 0. Assuming e is a free parameter, a value of 0.08 ± 0.12 is found. Our current data set does not significantly constrain the eccentricity. The final *rms* of the residuals is 77 m/s, a value close to individual error bars; the achieved reduced χ^2 is 1.25 when period, time, and eccentricity are fixed.

Common tests on the bisector behaviour have been performed, as shown in Figure 7. The bisector span is estimated between the wings and the core of the cross-correlation function, and its behaviour as a function of the radial velocities and the residuals to the Keplerian fit are examined.

No trend is found between the bisector span and the velocity, with a correlation coefficient of 7%; this indicates a low probability of a triple system or a diluted binary scenario. A slight trend (correlation of 41%) is observed between the bisector slope and the residuals to the fit. However, as suggested in Figure 7, this bisector behaviour is dominated by the data that have the lowest signal-to-noise ratios. This test shows the limitation of the bisector diagnostics, when the wings of the cross-correlation function are strongly affected by the spectrum continuum, at SNR typically less than ~ 5 . Because the bisector has no detected variation in phase with the radial-velocity variations, we conclude that the scenario involving a transiting planetary companion of CoRoT-17 is the only explanation for the observed radial velocity variations.

3.3. Spectral analysis of the host star

As part of the NASA's key science programme in support of the CoRoT mission, CoRoT-17 was also observed on 2010 June 20 (UT) with the HIRES spectrograph (Vogt et al. 1994) mounted on the Keck I 10 m telescope, at the Keck Observatory (Mauna Kea, Hawai'i). The red cross-disperser along with the 0'.861 wide slit and 14'' tall decker were employed to properly subtract the sky background, yielding a resolving power of $R \approx 50\,000$ and a wavelength coverage $3800 \leq \lambda \leq 7975$ Å. Six consecutive spectra of 1200 sec each were acquired to increase the S/N ratio and remove cosmic ray hits. The spectra were extracted and co-added with standard IRAF routines, giving a final S/N ratio of about 65 at 6000 Å.

Following the standard practice already adopted in previous CoRoT discovery papers (e.g., Deleuil et al. 2008; Fridlund et al. 2010; Gandolfi et al. 2010), we used a HIRES co-added spectrum to derive the fundamental physical parameters of CoRoT-17, i.e., effective temperature (T_{eff}), surface gravity ($\log g$),

Table 4. HARPS radial-velocity measurements of CoRoT-17

hline BJD-24500000.	RV	σ_{RV}	BIS
(days)	[km/s]	[km/s]	[km/s]
55326.90632	54.548	0.055	0.044
55340.87074	54.929	0.086	-0.054
55342.89312	54.553	0.101	-0.060
55351.86818	55.062	0.090	0.071
55352.64808	54.876	0.089	-0.141
55353.64740	54.630	0.085	0.273
55354.82094	54.734	0.087	0.231
55355.64015	55.212	0.101	0.189
55359.62782	54.970	0.081	-0.026
55372.76478	54.498	0.071	0.051
55387.68993	54.404	0.060	0.103
55396.65855	54.952	0.120	-0.173
55399.62341	54.543	0.067	-0.040
55407.67391	54.970	0.065	0.101
55409.67746	54.540	0.056	0.082
55412.66468	55.112	0.095	0.028
55427.58796	55.013	0.076	0.065

metallicity ([Fe/H]), and projected rotational velocity ($v \sin i$). Some methods consist of comparing the observed spectra with a grid of model atmospheres from Castelli & Kurucz (2004), Coelho et al. (2005) and Gustafsson et al. (2008), using spectral lines that are sensitive to the different photospheric parameters. Other methods rely on the use of spectral analysis packages like SME 2.1 (Valenti & Piskunov 1996; Valenti & Fischer 2005) and VWA (Bruntt et al. 2004, 2008, 2010). We found consistent results regardless of the spectrum and procedure. The final values adopted for the above mentioned physical parameters are $T_{\text{eff}} = 5740 \pm 80$ K, $\log g = 4.40 \pm 0.10$, $[\text{Fe}/\text{H}] = 0.0 \pm 0.1$, and $v \sin i = 4.5 \pm 0.5$ km/s (Table 2).

Using the $M_{\text{star}}^{1/3}/R_{\text{star}}$ value obtained from the transit light curve modelling, we obtained the mass, radius, and age of the host star via the same procedure we applied in earlier CoRoT planet-detection publications (see e.g. Deleuil et al. 2008). The results are reported in Table 2. Note that the star is quite evolved from the ZAMS, and based on the presently available constraints (effective temperature, metallicity, $M_{\text{star}}^{1/3}/R_{\text{star}}$ parameter), we found the age of the star to be 10.7 ± 1.0 Gyr.

3.4. The spectral energy distribution of the host star

The interstellar extinction (A_V) and distance (d) to the star were derived using the $r'i'JHKs$ photometry from the ExoDat database combined with IRAC@Spitzer 3.6, 4.5, 5.8, and 8.0 μm magnitudes (Table 1). The Spitzer-magnitudes were extracted by applying aperture photometry on the IRAC image cut-outs centred around CoRoT-17, as retrieved from the IRSA-NASA/IPAC Infrared Science Archive². Following the method described in Gandolfi et al. (2008), we simultaneously fitted the colours encompassed by the spectral energy distribution (SED, see Figure 8) with synthetic magnitudes derived from the *NextGen* stellar atmosphere model (Hauschildt et al. 1999) with the same T_{eff} , $\log g$, and [Fe/H] as the star. Assuming a normal total-to-selective extinction coefficient ratio $R_V = 3.1$ and a black body emission at the star's effective temperature and radius, we found $A_V = 2.60 \pm 0.10$ mag and $d = 920 \pm 50$ pc. The IRAC 5.8 and 8.0 μm images reveal a patchy nebula spatially projected towards the direction of CoRoT-17. The presence of foreground interstellar medium for such a low galactic latitude

² <http://irsa.ipac.caltech.edu/>

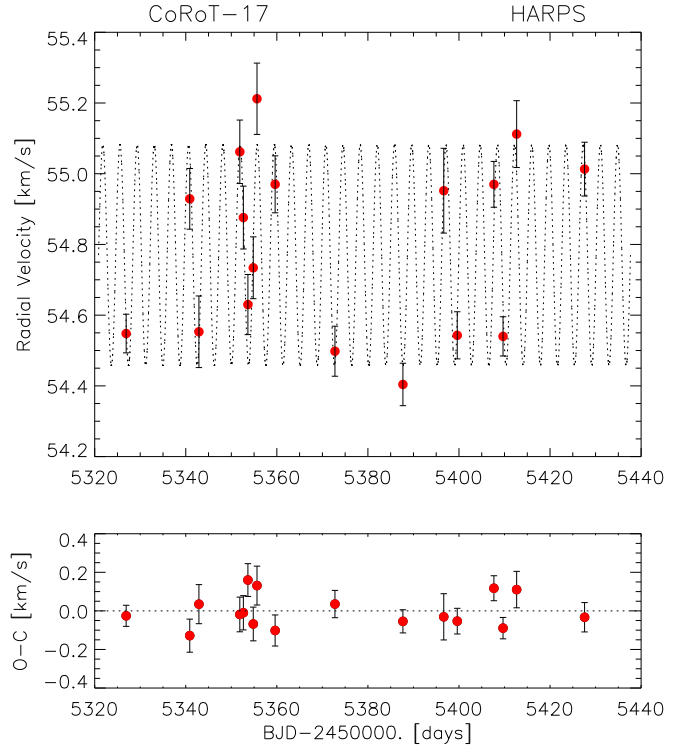


Fig. 5. Radial-velocity variations of CoRoT-17 obtained with HARPS as a function of time. The Keplerian best fit is superimposed. The bottom plot shows the residuals to this model.

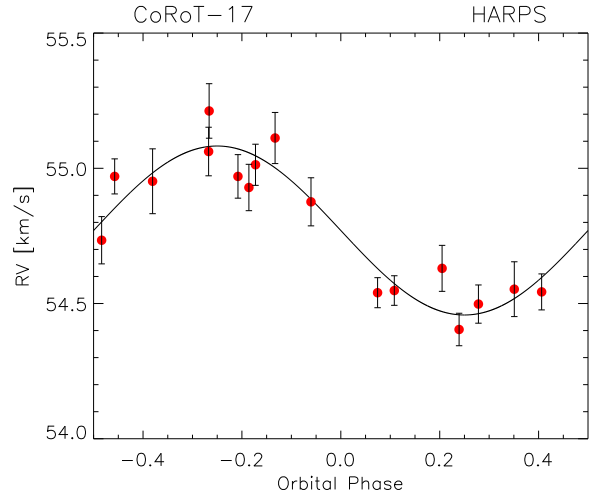


Fig. 6. RV data of CoRoT-17 folded to the ephemeris derived from CoRoT transits.

star ($b \approx 0.7^\circ$) might account for the derived high extinction value.

4. Discussion

We reported the discovery of a transiting exoplanet around the faint star CoRoT-17, detected by the CoRoT satellite. Extensive radial velocity, spectroscopic and photometric follow-up measurements proved that the cause of these transits is a transiting exoplanet that orbits the star. The measurements also helped to determine the basic characteristics of this planetary system.

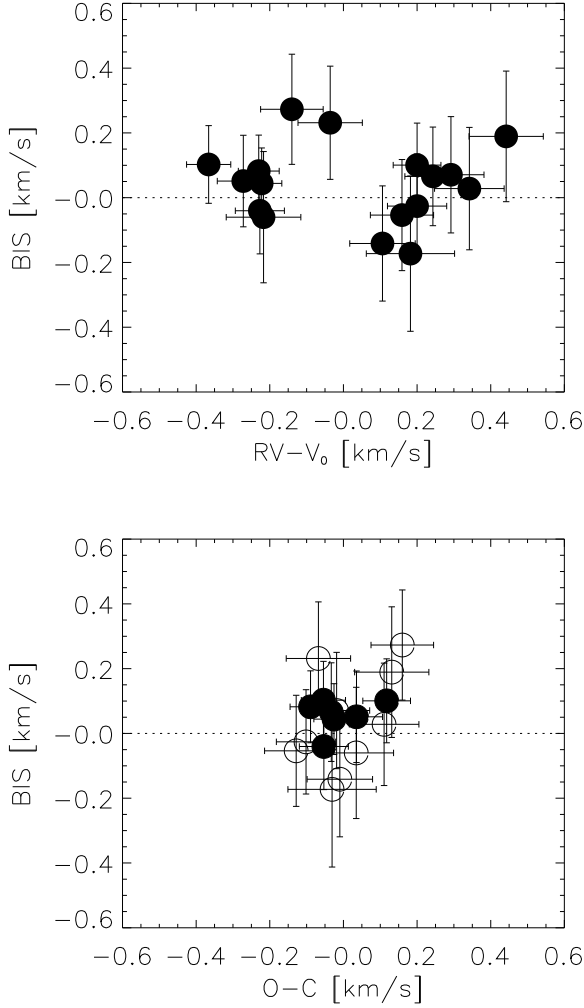


Fig. 7. Variations of the bisector span of CoRoT-17 RV data as a function of the measured velocities (top) and the residuals to the Keplerian fit (bottom). The first plot shows no correlation, a good indication for the planetary hypothesis as opposed to a blend binary signal. The second plot shows a weak correlation, owing the lowest SNR data of the sample (open points show the data where SNR is less than 5).

The planet has a mass of $2.43 \pm 0.30 M_{\text{Jup}}$ and a radius of $1.02 \pm 0.07 M_{\text{Jup}}$, while the mean density is $2.82 \pm 0.38 \text{ g/cm}^3$ (Table 2). The transit is almost central and it has 0.44% depth, but the CoRoT light curve is contaminated by another star, which contributes $8 \pm 4\%$ to the total observed flux. The host star is an evolved G2V type star, with mass $1.04 \pm 0.10 M_{\odot}$ and radius $1.59 \pm 0.07 R_{\odot}$. The isochrone fit yielded the age of the star, which is 10.7 ± 1.0 Gyr. This makes the system one of the oldest known systems among the transiting exoplanets.

CoRoT-17b is located in a quite common place on the mass – radius diagram of the known transiting exoplanets (see e.g. Southworth 2010; Swift et al. 2010). To probe the possible composition of CoRoT-17b, we computed stellar and planetary evolution models using PADOVA (Marigo et al. 2008; Bertelli et al. 2008) and CEPAM (Guillot & Morel 1995), as described in Guillot & Havel (2011). The results are shown in Fig 9 where the evolution of the size of CoRoT-17b is plotted as a function of the system age. The colours indicate the distance in

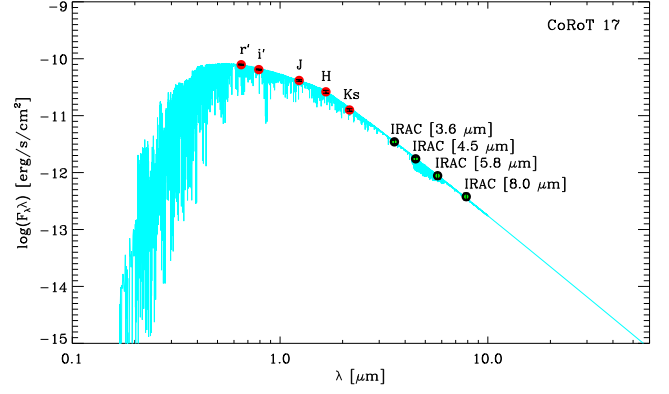


Fig. 8. Spectral energy distribution of CoRoT-17. Dereddened $r'i'JHKs$ and IRAC infrared data are represented with filled red and green dots, respectively. The model spectrum by Hauschildt et al. (1999) with the same temperature, radius, and metallicity as CoRoT-17 are plotted with a light-blue line.

standard deviations from the inferred effective temperature and mean stellar density, i.e., less than 1σ (green), 2σ (blue) and 3σ (yellow). These constraints are compared to planetary evolution models for a homogeneous solar-composition hydrogen-planet, with different hypotheses: (plain lines) using a 'standard model', i.e., without additional sources of heat; (dotted lines) by adding a fraction (0.25%) of the incoming stellar energy and dissipating it at the centre. These two cases correspond to standard recipes used to explain the inflated giant exoplanets (Guillot 2008). In this context, it is hard to constrain the mass of heavy elements needed to match the observed planetary radius. The core mass can range from 0 (pure H-He planet) to ~ 380 earth-masses ($\sim 48\%$ of the total mass), depending on the hypothesis we consider. However, this diagram is not sensitive for the properties of CoRoT-17b, because - depending on the assumptions - we can easily construct models with 192 and $384 M_{\text{earth}}$ of heavy elements inside the planet, too, which are practically undistinguishable at the age of the system, because at very late stages of planetary evolution these two evolutionary tracks are closer to each other than the uncertainty in the planetary radius.

Similarly to other known old planetary systems (e.g. HAT-P-21, 10.2 ± 2.5 Gyr, and HAT-P-22, 12.4 ± 2.6 Gyr, see Bakos et al. (2010)), CoRoT-17 has an age that is inferred to be 10.7 ± 1.0 Gyr. Its present bolometric luminosity is about $2.47 L_{\odot}$, implying that as the star is evolving, the planet is receiving more energy. With an equilibrium temperature of ~ 1600 K, the planet still appears to be safe in terms of evaporation, however, and any possible increase of its radius should remain very limited.

A star with $\sim 1.0 M_{\odot}$ spends approximately 10-11 Gyr on the main sequence. Stellar evolution studies predict that a star similar to CoRoT-17 reaches its present radius at $\sim 90\%$ of its main-sequence lifetime (Hurley et al. 2000), depending on its metallicity and on its exact mass. The present orbital radius of the planet is $9.95 R_{\odot}$, whereas we expect the star in its giant phase to reach well over $150 R_{\odot}$. Even if the star loses mass owing to winds, the engulfment of the planet seems inevitable (see e.g. Rasio et al. 1996).

Acknowledgements. The team at IAC acknowledges support by grant ESP2007-65480-C02-02 of the Spanish Ministerio de Ciencia e Innovación. This research has made use of the ExoDat database, operated at LAM-OAMP, Marseille, France, on behalf of the CoRoT/Exoplanet program. This publication makes use of data products from the Two Micron All Sky Survey, which is a joint project of the University of Massachusetts and the Infrared Processing and Analysis Center/California Institute of Technology, funded by the National Aeronautics

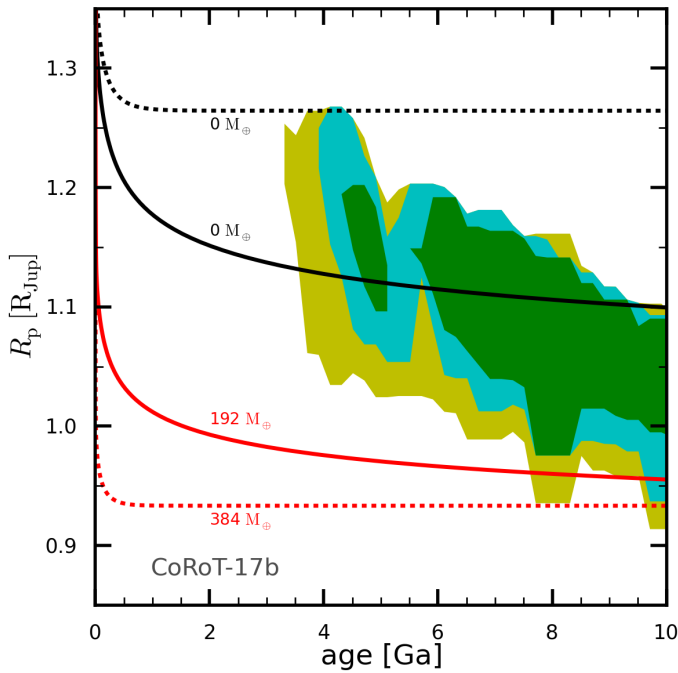


Fig. 9. Evolution of the size of CoRoT-17b (radius in Jupiter units) as a function of age (in billion years), compared to constraints inferred from CoRoT photometry, spectroscopy, radial velocimetry, and the PADOVA stellar isochrones. Green, blue, and yellow-green plain regions correspond to the planetary radii and ages that result from stellar evolution models that match the inferred $\rho_{star} - T_{eff}$ uncertainty ellipse within 1, 2, and 3σ , respectively. Planetary evolution models for a planet with a solar-composition envelope and no dissipation are shown as plain lines and labelled according to the value of the core mass (in earth masses); models in which 0.25% of the incoming flux is deposited at the planet's centre are shown as dotted lines. Models with no core are shown in black, and with a core in red. These models assume a total mass of $2.43M_{Jup}$ and an equilibrium temperature of 1626 K.

and Space Administration and the National Science Foundation. This research has made use of NASA's Astrophysics Data System. TRAPPIST is a project funded by the Belgian Fund for Scientific Research (Fond National de la Recherche Scientifique, FNRS) under the grant FRFC 2.5.594.09.F, with the participation of the Swiss National Science Foundation (SNF). M. Gillon and E. Jehin are FNRS Research Associates. M. Endl, W.D. Cochran and P.J. MacQueen were supported by NASA Origins of Solar Systems grant NNX09AB30G. The German CoRoT Team (TLS and the University of Cologne) acknowledges DLR grants 50 OW 204, 50 OW 0603 and 50QP07011.

References

- Auvergne, M., Bodin, P., Boissard, L., et al. 2009, *A&A* 506, 411
 Bakos, G. Á., Hartman, J., Torres, G., Latham, D. W., Kovács, G. et al. arXiv:1008.3388
 Baglin, A., Auvergne, M., Barge, P., et al. 2007, in American Institute of Physics Conference Series, 895, ed. C. Dumitrache, N. A. Popescu, M. D. Suran, & V. Mioc, 201
 Baranne, A., Queloz, D., Mayor, M., et al. 1996, *A&AS* 119, 373
 Batten, A. H. 2005, *Ap&SS* 296, 3
 Baudin, F., Jorda, L., Samadi, R., Michel, E. 2008, "N2 data: description", available at: <http://idoc-corotn2-public.ias.u-psud.fr/jsp/CorotHelp.jsp>
 Bertelli, G., Girardi, L., Marigo, P. Nasi, E. *A&A* 484, 815
 Boissard, L., Baglin, A., Auvergne, M., Deleuil, M., Catala, C. 2006, in ESA SP, 1306, 465
 Bordé, P., Bouchy, F., Deleuil, M., Cabrera, J., Jorda, L. et al. 2010, *A&A* 520, A66

- Bouchy, F., Moutou, C., Queloz, D. and the CoRoT Exoplanet Science Team 2009, *IAUS* 253, 129
 Brown, T. M., Charbonneau, D., Gilliland, R. L., Noyes, R. W., Burrows, A. 2001, *ApJ* 552, 699
 Bruntt, H., Bikmaev, I. F., Catala, C., et al. 2004, *A&A*, 425, 683
 Bruntt, H., De Cat, P. & Aerts, C. 2008, *A&A*, 478, 487
 Bruntt, H., Deleuil, M., Fridlund M. et al. 2010, *A&A* 519, 51
 Castelli, F. & Kurucz, R.L. 2004, eprint arXiv:astro-ph/0405087
 Coelho, P., Barbuy, B., Meléndez, J., et al. 2005, *A&A* 443, 735
 Deeg, H. J., Gillon, M., Shporer, A. et al. 2009, *A&A* 506, 343
 Deleuil, M., Deeg, H. J., Alonso, R., Bouchy, F., Rouan, D. et al. 2008, *A&A* 491, 889
 Deleuil, M., Meunier, J. C., Moutou, C., et al. 2009, *AJ*, 138, 649
 Erikson et al. 2011, in prep.
 Fridlund, M., Hébrard, G., Alonso, R., Deleuil, M., Gandolfi, D. et al. 2010, *A&A* 512, A14
 Gandolfi, D. et al. 2008, *ApJ* 687, 1303
 Gandolfi, D., Hébrard, G., Alonso, R., Deleuil, M., Guenther, E. W. et al. 2010, *A&A* 524, A55
 Geem, Z. W., Kim, J. H., Lonatathan, G. V. 2001, *Simulation*, 76, 60
 Gillon, M., Jehin, E., Magain, P., Chantry, V., Hutsemekers, D., Manfroid, J., Queloz, D., Udry, S. 2011, 'TRAPPIST: a robotic telescope dedicated to the study of planetary systems', in: *Detection and Dynamics of Transiting Exoplanets*, Proceedings of Haute-Provence Observatory Colloquium (23-27 August 2010), Edited by F. Bouchy, R.F. Díaz & C. Moutou
 Guillot, T. 2008, *PhST* 130, 4023
 Guillot, T., Morel, P. 1995, *A&AS* 109, 109
 Guillot, T., Havel, M. 2011, *A&A* 527, 20
 Gustafsson, B., Edvardsson, B., Eriksson, K., et al. 2008, *A&A*, 486, 951
 Hirschfeld, P. H., Allard, F., Baron, E. 1999, *ApJ* 512, 377
 Hurley, J. R., Pols, O. R., Tout, Ch., A. 2000, *MNRAS* 315, 543
 Mandel, K., Agol, E. 2002, *ApJ* 580, L171
 Mayor, M., Pepe, F., Queloz, D., Bouchy, F., Rupprecht et al. 2003, *Msngr* 114, 20
 Marigo, P., Girardi, L., Bressan, A., Groenewegen, M. A. T., Silva, L. Granato, G. L. *A&A* 482, 883
 Pepe, F., Rupprecht, G., Avila, G. et al. 2003, *SPIE* 4841, 1045
 Quentin, C. G., Barge, P., Cautain, R., Meunier, J.-C., Moutou, C., Savalle, R., Surace, C. 2006, *ESASP* 1306, 409
 Rasio, F. A., Tout, C. A., Lubow, S. H., Livio, M. 1996 *ApJ* 470, 1187
 Roberts, A. 1899, *ApJ* 10, 308
 Russell, H. M. 1932, Annual report of the Smithsonian Institute 1931
 Sing, D. K. 2010, *A&A* 510, 21
 Southworth, J. 2010, *MNRAS* 408, 1689
 Surace, C., Alonso, R., Barge, P. et al. 2008, in *SPIE Conf. Ser.*, 7019
 Swift, D. Eggert, J., Hicks, D. Hamel, S. Caspersen, K., Schwegler, E., Collins, G., Ackland G. 2010, arXiv:1001.4851
 Valenti, J. A. & Piskunov, N., 1996, *A&AS*, 118, 595
 Valenti, J. A. & Fischer, D. A., 2005, *ApJS*, 159, 141
 Vogt, S. S., Allen, S. L., Bigelow, B. C. et al. 1994, *SPIE* 2198, 362
 Winn, J. N. 2010, 'Transits and Occultations', arXiv.org:1001.2010

-
- ¹ Institute of Planetary Research, German Aerospace Center, Rutherfordstrasse 2, 12489 Berlin, Germany
 - ² Laboratoire d'Astrophysique de Marseille, 38 rue Frédéric Joliot-Curie, 13388 Marseille cedex 13, France
 - ³ LUTH, Observatoire de Paris, UMR 8102 CNRS, Université Paris Diderot; 5 place Jules Janssen, 92195 Meudon, France
 - ⁴ Research and Scientific Support Department, ESTEC/ESA, PO Box 299, 2200 AG Noordwijk, The Netherlands
 - ⁵ Department of Physics, Denys Wilkinson Building Keble Road, Oxford, OX1 3RH, UK
 - ⁶ Observatoire de l'Université de Genève, 51 chemin des Maillettes, 1290 Sauverny, Switzerland
 - ⁷ LESIA, UMR 8109 CNRS, Observatoire de Paris, UPMC, Université Paris-Diderot, 5 place J. Janssen, 92195 Meudon, France
 - ⁸ Institut d'Astrophysique Spatiale, Université Paris XI, F-91405 Orsay, France
 - ⁹ McDonald Observatory, University of Texas at Austin, Austin, 78712 TX, USA
 - ¹⁰ Instituto de Astrofísica de Canarias, E-38205 La Laguna, Tenerife, Spain
 - ¹¹ Universidad de La Laguna, Dept. de Astrofísica, 38200 La Laguna, Tenerife, Spain
 - ¹² Observatoire de Haute Provence, 04670 Saint Michel l'Observatoire, France
 - ¹³ Institut d'Astrophysique de Paris, UMR 7095 CNRS, Université Pierre & Marie Curie, 98bis boulevard Arago, 75014 Paris, France
 - ¹⁴ Rheinisches Institut für Umweltforschung an der Universität zu Köln, Aachener Strasse 209, 50931, Germany
 - ¹⁵ University of Vienna, Institute of Astronomy, Türkenschanzstr. 17, A-1180 Vienna, Austria
 - ¹⁶ IAG-Universidade de Sao Paulo, Brasil
 - ¹⁷ Université de Nice-Sophia Antipolis, CNRS UMR 6202, Observatoire de la Côte d'Azur, BP 4229, 06304 Nice Cedex 4, France
 - ¹⁸ University of Liège, Allée du 6 août 17, Sart Tilman, Liège 1, Belgium
 - ¹⁹ Thüringer Landessternwarte, Sternwarte 5, Tautenburg 5, D-07778 Tautenburg, Germany
 - ²⁰ Space Research Institute, Austrian Academy of Science, Schmiedlstr. 6, A-8042 Graz, Austria
 - ²¹ School of Physics and Astronomy, Raymond and Beverly Sackler Faculty of Exact Sciences, Tel Aviv University, Tel Aviv, Israel
 - ²² Center for Astronomy and Astrophysics, TU Berlin, Hardenbergstr. 36, 10623 Berlin, Germany